Electronic structure of boron nitride single crystals and films

J. B. MacNaughton, A. Moewes, and R. G. Wilks
Department of Physics and Engineering Physics, University of Saskatchewan, 116 Science Place, Saskatoon, Saskatchewan S7 N 5E2, Canada

X. T. Zhou and T. K. Sham
Department of Chemistry, University of Western Ontario, London, Ontario N6A 5B7, Canada

T. Taniguchi and K. Watanabe
Advanced Materials Laboratory, National Institute for Material Science, 1-1 Namiki, Tsukuba, 305-0044, Japan

C. Y. Chan, W. J. Zhang, I. Bello, and S. T. Lee
Center of Super-Diamond and Advanced Films (COSDAF) and Department of Physics and Materials Science, City University of Hong Kong, Hong Kong SAR, China

H. Hofsäss
II. Institute of Physics, University of Göttingen, Friedrich-Hund-Platz 1, D-37077, Göttingen, Germany
(Received 5 August 2005; revised manuscript received 5 October 2005; published 23 November 2005)

We present a comparison between experimental soft x-ray spectra and density of states calculations of hexagonal boron nitride (*h*-BN) and cubic boron nitride (*c*-BN) single crystals. Cubic boron nitride films, grown on both mirror and scratched single crystal silicon wafers, have also been investigated using soft x-ray absorption spectroscopy (XAS) and soft x-ray emission spectroscopy (XES). Spectra measured at the 1*s* thresholds of boron and nitrogen give a complete picture of the occupied and unoccupied partial density of states for these materials. The films are shown to be a mixture of sp^3 bonded nanocrystalline *c*-BN phase and sp^2 bonded *h*-BN phase. As the roughness of the deposition surface increases, a decrease in the amount of sp^3 phase in the resulting film is observed. There are clear differences between the electronic structures of the nanocrystalline films and the single crystal samples. No differences between the spectra of the single crystals and previously reported measurements on powder samples of BN were observed.

DOI: 10.1103/PhysRevB.72.195113 PACS number(s): 78.70.En, 78.70.Dm, 71.20.−b, 73.61.−r

I. INTRODUCTION

Boron nitride (BN) has been the subject of numerous theoretical and experimental studies. The most common crystal structures of BN are cubic and hexagonal, although several others can be formed. The hexagonal phase (*h*-BN) is a layered, sp^2-bonded material, isostructural to graphite. In contrast to graphite, which exhibits semimetallic behavior, *h*-BN is a wide gap semiconductor. Hexagonal boron nitride crystals demonstrate both high chemical and thermal stabilities, which indicates that they have applications as optical devices or sensors that can operate under high pressure and/or high temperature.[1] The electronic properties of *h*-BN suggest that it may also be useful in the production of a compact ultraviolet laser device that could be used in optical storage, photocatalysis, sterilization, ophthalmic surgery, and nanosurgery applications.[2]

The cubic phase (*c*-BN) has a zinc-blende lattice structure with sp^3-hybridized B-N bonds. Boron nitride in this form has a variety of interesting properties, including being ultrahard, as well as having a high melting point and high thermal conductivity.[3] Cubic BN has a similar structure to diamond, although, unlike diamond, *c*-BN is not reactive with ferrous materials up to high temperatures, and it has the ability to form both *n*- and *p*-type semiconductors when doped appropriately.[4] For industrial tools used in cutting and shaping iron- or nickel-containing materials, *c*-BN is superior to diamond, as the *c*-BN blades do not deteriorate as a result of reactions with this sort of material.[5] Cubic boron nitride thin films are also of interest, as they are an ideal for use as a protective coating on steel. Such films may also be used in the construction of field emitting devices, because *c*-BN can be *n* doped with silicon and the *c*-BN surface can have a negative electron affinity.[6]

These samples have had previous theoretical investigations of their electronic structure[7–11] and have been examined with soft x-ray absorption spectroscopy (XAS), x-ray emission spectroscopy (XES), and resonant inelastic x-ray scattering (RIXS).[12–24] More specifically, x-ray absorption spectroscopy has been used to examine the differences in bonding configurations between *c*-BN, *h*-BN, and BN thin films.[15,18,20,21] Several studies have specifically targeted boron $K\alpha$ x-ray emission of polycrystalline and powdered *h*-BN, investigating and identifying the features of the emission spectra when exciting nonresonantly, resonantly and just below the *K* edge.[13,17,19,23,25] The nitrogen edge of powdered *h*-BN has been studied,[24] and both N and B edges have been investigated for a *c*-BN crystal.[22] Furthermore, the characteristics of the substrate have been shown to be an important factor that influences the *c*-BN films being deposited.[26] Specifically, a study involving *c*-BN films deposited by an arc-like plasma enhanced ion plating technique demonstrated

 ©2005 The American Physical Society

that a rougher silicon substrate will result in the decrease of the volume ratio of *c*-BN in the film as compared to a film deposited on mirror silicon.[27]

Despite the extensive studies of these materials, the sizes and characteristics of their band gaps are subjects of controversy.[1,2,7,8,12,22,28–30] Measured values of the size of the energy gap range from 3.6 to 7.1 eV for *h*-BN.[30] There is less disagreement regarding the energy gap value of *c*-BN; it is agreed that it is approximately 6.2 eV.[1,12,22] Theoretically predicted values of the energy gap of *c*-BN, however, are significantly larger.[8,28] One theory that attempts to explain the observed discrepancies claims that the poor crystalline quality of the samples that were measured led to variations in the gathered data, and so a technique for synthesizing pure crystalline samples of both *c*-BN and *h*-BN has been developed.[1,2,31]

In the following sections, soft x-ray spectroscopic measurements at the boron and nitrogen *K* edges of very high quality single crystals of *h*-BN and *c*-BN will be presented and compared to the results of our density of states calculations. The goal is to obtain a complete picture of the electronic states of different BN structures and to compare them to those of thin BN films. In addition, a spectroscopic examination of the effects of surface roughness on the electronic structure of the thin films of *c*-BN will be presented.

II. SAMPLE SYNTHESIS

Single crystals of both hexagonal and cubic boron nitride are obtained using a carefully purified Ba-B-N solvent system for the temperature gradient method using a modified belt-type apparatus with a bore diameter of 60 mm, under both high-pressure and high-temperature (HP-HT).[32] The source used for BN were a *h*-BN rod (Shin-etsu Kagaku Co. Ltd., type KD-3S) and a powder [Shin-etsu Kagaku Co. Ltd., type KBN-(h)10]. During sample synthesis, the growth cell containing a mixture of the barium-BN system and *h*-BN powder tends to become contaminated with oxygen. To reduce these effects, the growth cell was carefully prepared in a box with a nitrogen atmosphere, keeping the levels of O_2 and H_2O below 1 ppm. The powder *h*-BN was deoxidized by heating to 2100 °C for 2 h under vacuum (10^{-3} Pa). After the heat treatment, the oxygen content of the *h*-BN source was measured to be about 0.06 wt. % by an oxygen analyzer (Horiba Co. Ltd., EMGA-650). The solvent used for this procedure was barium boron nitride ($Ba_3B_2N_4$), synthesized by the reaction of barium nitride and BN at 1000 °C under dry nitrogen atmosphere. A molybdenum (Mo) sample chamber was used for the growth experiments. The assembled growth cell was compressed under 4.5–5.5 GPa and was subsequently heated to 1500–1750 °C, facilitating the growth of nucleated *c*-BN crystals and recrystallized *h*-BN crystals. The holding time for the growth was varied from 20 to 80 h. Although there was a temperature gradient in the sample chamber, the growth temperature denoted in this study corresponds to the temperature of the central portion of the furnace near the region of the BN source. After these HP-HT experiments, the recovered Mo sample chamber was dissolved using hot aqua regia and the grown crystals were obtained. The crystals that were produced were colorless, transparent and 1–6 mm^2 in size. The detailed experimental procedure has been described elsewhere.[1,32,33] The minimal amount of defects in these samples will ensure an accurate experimental study of the electronic structure.

Many methods for producing thin films of *c*-BN have been developed. Plasma assisted chemical vapor deposition (CVD), laser ablation, ion-beam deposition, and sputtering[34–37] are all common techniques used for this purpose. All of these techniques involve the growth of *c*-BN films using bombardment with energetic ions. The films that are the result of many of these processes are nanocrystalline and contain a mixture of *h*-BN (sp^2 bonding) and *c*-BN (sp^3 bonding) phases. The crystal size and the ratio of *c*-BN to *h*-BN are influenced by the deposition technique and the parameters used during production. The mass-selected ion beam deposition (MSIBD) technique was used by Hofsäss *et al.* to deposit *c*-BN films.[34] This technique has well defined conditions, and only the selected ions ($^{11}B^+$ and $^{14}N^+$) are allowed to participate in the nucleation and growth process, ensuring that no contaminating species play a role in the deposition. Using this procedure, thin films with high *c*-BN content can be obtained.[34] In addition to being influenced by the synthesis technique and deposition parameters, the characteristics and composition of the deposited films are also affected by the roughness of the substrate on which they are deposited.[38] The films measured in this study were grown using the MSIBD technique on mirror silicon wafers, as well as on single-crystal silicon wafers that had been scratched with diamond particles (particle sizes of 0.25, 1, and 3 μm) prior to deposition.

Taniguchi's research group synthesized the samples of purified single crystals of *h*-BN and *c*-BN used in this study. The *c*-BN films were produced by Lee and Hofsäss's group and were provided by Sham's research group.

III. EXPERIMENT

Beamline 8.0.1 at the Advanced Light Source synchrotron at Lawrence Berkeley National Laboratory was used for the soft x-ray spectroscopic measurements. The x-ray absorption spectra of all samples were measured in total electron yield (TEY) mode. The energy resolution for the absorption spectra is around 40 and 80 meV for the nitrogen and boron edges, respectively. For the fluorescence spectra, the emitted radiation is partially collected by a Rowland circle-type spectrometer with interchangeable spherical gratings and recorded with an area-sensitive multichannel detector. The details of this endstation are described elsewhere.[39] Total experimental resolution in the $K\alpha$ x-ray emission region is 0.3 eV full width at half maximum (FWHM) for boron and 0.75 eV FWHM for nitrogen. All absorption and emission spectra are normalized to the number of photons falling on the sample, monitored by a highly transparent gold mesh in front of the sample. The energy axes of the obtained absorption and emission spectra have been calibrated according to the values for *h*-BN reported by Fomichev *et al.*[12]

IV. CALCULATIONS

Density functional theory calculations utilizing generalized gradient approximations[40] (GGA) of the exchange and

correlation energies were used to model the electronic structures of *c*-BN and *h*-BN. The WIEN2K (Ref. 41) software was used for these calculations; it utilizes the full potential (linearized) augmented plane wave+local orbitals (L/APW +LO) method[42,43] within the Kohn-Sham framework to describe the system. The unit cell is split into regions described by nonoverlapping atomic spheres centred on each atom as well as an interstitial region surrounding the spheres. Inside the spheres, basis sets consist of a linear combination of radial functions multiplied by spherical harmonics, while a plane wave expansion is used in the interstitial region.[43] The former functions are solutions of the radial Schrödinger equation for fixed energy and given angular momentum. The DFT scheme used by WIEN2K uses a fixed linearization energy but also takes into account energy dependence by using a k_n-independent local orbital.[43]

The zinc-blende structure of *c*-BN is well known and has the space group $F\bar{4}3m$, or No. 216. The lattice parameter used was $a=3.615$ Å for the calculation of *c*-BN.[9] Hexagonal boron nitride has been reported to form into 5 very similar structures,[7] the most commonly accepted of which is $P6_3/mmc$, or No. 194. It is this structure that has been chosen for the density of states calculations in this study. The lattice parameters $a=2.50441$ Å and $c=6.6522$ Å were used for the calculation of the *h*-BN electronic structure.[7] These structures and space groups represent the only significant input for the WIEN2K program.

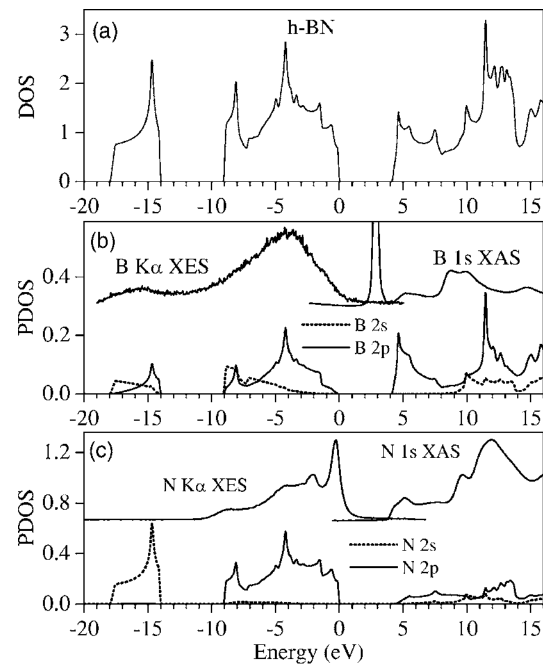

FIG. 1. Comparison of (a) total density of states, (b) calculated boron $2p$ and $2s$ partial density of states and experimental B $K\alpha$ XES and B $1s$ XAS, and (c) calculated nitrogen $2p$ and $2s$ partial density of states and experimental N $K\alpha$ XES and N $1s$ XAS of *h*-BN.

V. RESULTS AND DISCUSSION

Figure 1 displays the calculated density of states and the soft x-ray spectroscopic results for hexagonal boron nitride. The total DOS calculated by the WIEN2K program is displayed in part (a), while the partial DOS of the boron and nitrogen edges are shown in parts (b) and (c), respectively, together with the measurements. Both the $2s$ and $2p$ contributions are shown for all edges. The results of the calculations are quite similar to those presented in previous studies of this material.[9] The comparison of the DOS with the measured spectra is based on the knowledge that the occupied and unoccupied densities of states of a material are probed by XES and XAS, respectively. In order to facilitate this comparison, the energy axes of the experimental data were shifted such that their prominent features align with those in the calculated DOS. For the absolute absorption and emission energies see Figs. 3–6. Figure 1 shows that the occupied DOS is represented quite well by the measured emission spectra, which are dominated by $2p$ contributions. The dominance of these contributions is expected, because the spectroscopic measurements are governed by standard dipole selection rules, and involve radiative transitions between a $1s$ core level and a higher-lying energy state. It is clear from the calculations that the upper valence band is dominated by contributions from both B and N $2p$ states, and the lower valence band is comprised mainly of N $2s$ states. The sharp feature at the onset of the B $1s$ XAS spectrum is due to a strong π^* exciton.[23] Experiments have shown that core excitons are more strongly bound at cation sites than at anion sites in ionic solids, and so the presence of this core exciton at the boron edge is expected.[11] It has been shown that the inclusion of the core hole effects in the calculation of the B $1s$ x-ray absorption spectrum will reproduce this sharp excitonic feature, while the results from a non-interacting (one electron) model will not contain the strong π^* feature.[23] As expected, this feature is not present in our calculated electronic structure, because core hole effects are not included in the calculations. Since XAS measurements model the unoccupied DOS in the presence of the core hole that is produced by irradiation,[44] the inclusion of these effects in the calculations would have greatly improved the match between experiment and theory in this region.

The comparison between the calculated DOS of *c*-BN and the corresponding spectroscopic data is shown in Fig. 2. As was the case with *h*-BN, the calculated electronic structure is in agreement with previous studies of *c*-BN.[9] The agreement between the experimental XES and the calculated $2p$ density of states at both the boron and nitrogen edges is once again quite strong. The calculations reveal that the lower valence band is formed mainly by N $2s$ states and the upper valence band consist primarily of B and N $2p$ states. The prepeak structure in the *c*-BN B $1s$ XAS spectrum is of interest, as its origin is the subject of considerable controversy in the literature. Some authors have not observed this peak in their *c*-BN spectra,[15,21] and argue that it is a result of improper energy calibration and contamination with *h*-BN phases.[21] However, evidence of a core exciton band in *c*-BN has been reported.[3,12,22] When our measurements of the *c*-BN single crystal are compared to those found in previously published studies, it is clear that we have reproduced this core exciton feature. It is important to note that these peaks are not due to

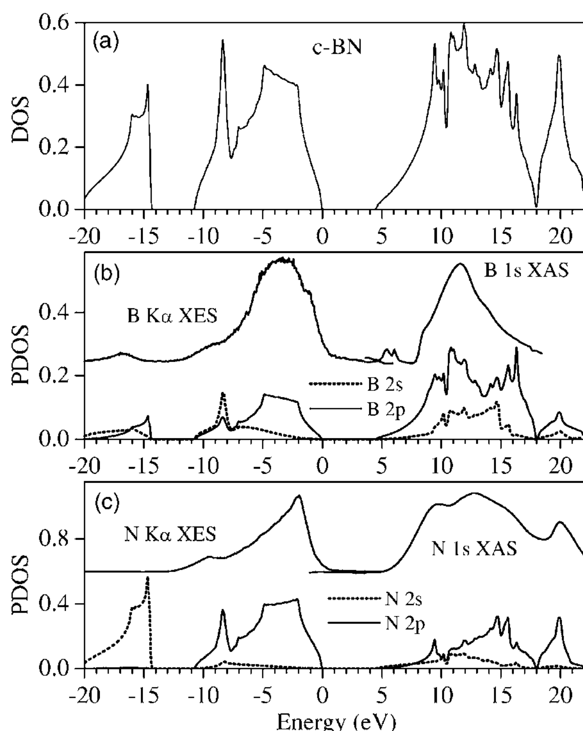

FIG. 2. Comparison of (a) total density of states, (b) calculated boron $2p$ and $2s$ partial density of states and experimental B $K\alpha$ XES and B $1s$ XAS, and (c) calculated nitrogen $2p$ and $2s$ partial density of states and experimental N $K\alpha$ XES and N $1s$ XAS of c-BN.

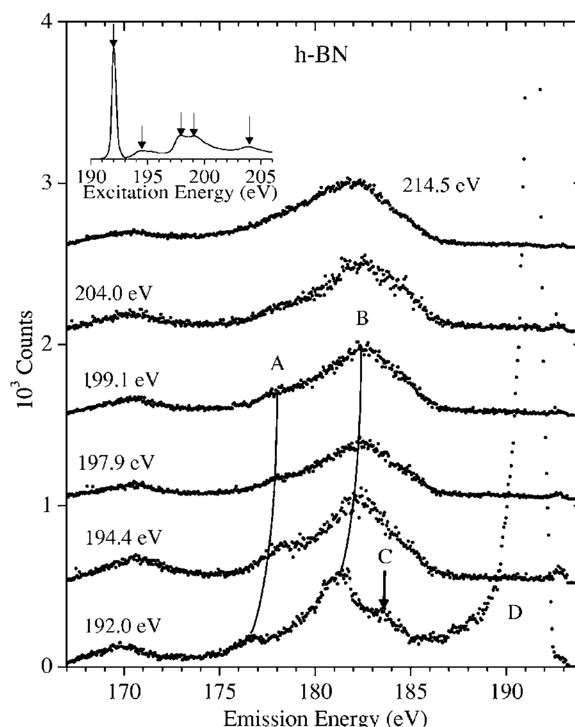

FIG. 3. Resonant boron $K\alpha$ emission of h-BN. The inset displays the B $1s$ XAS spectrum and the excitation energies used for the resonant emission spectra are indicated by arrows.

variations in the flux of the incoming photons introduced into the spectrum through the normalization process. Disagreement concerning the characteristics of this feature are seen, however, as our results show a distinct two-peak structure, while this feature has appeared as either a fairly broad, lower intensity peak[3,12] or as a single, very sharp narrow peak[22] in previous studies. Given the high purity of our single crystalline samples, we can rule out the possibility that the absorption prepeaks arise from contamination of c-BN with h-BN phases.

The set of resonantly excited B $K\alpha$ emission spectra of h-BN is shown in Fig. 3, with each spectrum's corresponding excitation energy displayed. The upper spectrum represents the nonresonant case, with the excitation energy well above the ionization threshold, while the other energies correspond to features in the B $1s$ XAS spectrum, shown in the inset. The evolution of the resonant spectra of this single crystal sample as a function of excitation energy is very similar to previously reported results for crushed powder samples.[19,23] The inelastic features A and B begin to track the excitation energy, as was previously observed. Feature C appears as a significant feature in the spectrum when the sample is excited at the threshold energy, and feature D stems from elastically scattered radiation and therefore corresponds to the energy of the incoming photons. Feature D is very strong when excited at 192.0 eV, presumably because the B $1s$ electron is excited into the π^* exciton state. Calculations have shown that the absorption is dominated by transitions from the B $1s$ core level to π^* states and the emission is dominated by transitions originating from σ states.[19] The energy loss features A and B correspond well with an electronic transition of valence band σ electrons to a π^* conduction band state; feature C may be an excitonic effect.[19] The shift in the features of the emission spectra has also been described as being the result of phonon relaxation and differences between initial and final state electronic screening.[25]

The resonant boron $K\alpha$ XES of c-BN is shown in Fig. 4. The excitation energies were chosen in the same manner as for the h-BN spectra, corresponding to features in the XAS spectrum displayed in the inset. As in Fig. 3, the highest excitation energy corresponds to the nonresonant case. The c-BN spectra show a clear dependence on the excitation energy, in agreement with the previously reported results.[22] Specifically, features B and C emerge as the excitation energy decreases toward the absorption threshold, while feature A experiences a decrease in intensity. In this case, feature D represents the elastically scattered incoming radiation. The excitation energies of the bottom two spectra correspond to the excitons discussed in the previous section, below the main boron absorption edge. The XES spectra become less intense at these energies, and the feature A can be seen to track the excitation energy. The energy separation between this inelastic loss feature and the elastic peak remains constant, similar to the behaviour of the features in the resonant spectra of h-BN. Features A, B, and C have been previously related to points of high symmetry in the band structure of c-BN.[22] Feature B is enhanced when the core electron is excited into the conduction band at a point where it has the same symmetry as the high symmetry point which is associated with feature B in the valence band. This point of high

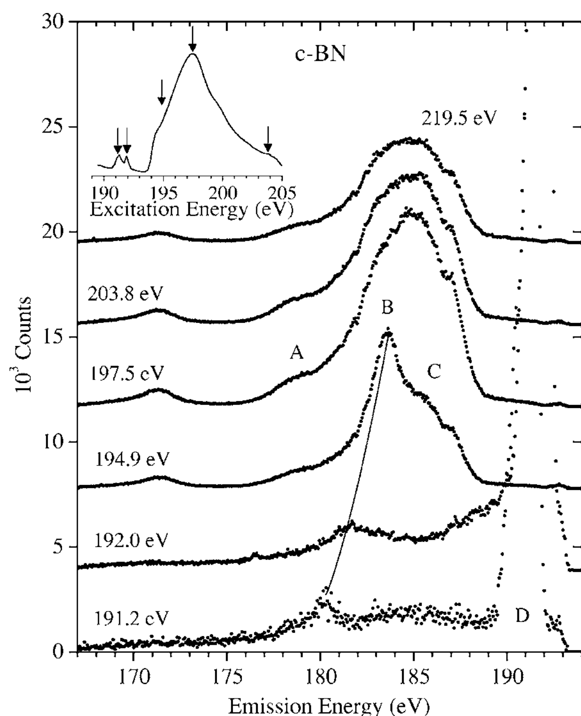

FIG. 4. Resonant boron $K\alpha$ emission of c-BN. The inset displays the B 1s XAS spectrum and the excitation energies used for the resonant emission spectra.

symmetry is an excitation to the lowest unoccupied band. This resonant behaviour in the emission process is the result of a momentum-conserved inelastic scattering process.

Figures 5 and 6 show the nitrogen $K\alpha$ RIXS for h-BN and c-BN, respectively. Similar to the boron edge spectra discussed above, the excitation energies correspond to features in the N 1s XAS absorption spectra and are displayed in the inset. In the h-BN spectra, feature D is associated with transitions from the N $2p_z$ states (π emission), while the 3 smaller peaks A, B, and C are attributed to the $2p_{xy}$ states (σ emission).[24] As the excitation energy is decreased, moving closer to the absorption threshold, the π emission becomes less pronounced. Very small changes are seen in the nitrogen spectra of c-BN excited at different resonant energies (Fig. 6).

The B 1s XAS of the c-BN films that were grown on mirror and scratched silicon (scratched with diamond particles of sizes of 0.25, 1, and 3 μm prior to film deposition) are compared to the XAS spectra of the single crystals of c-BN and h-BN in Fig. 7. The prominent feature A that is seen in all spectra is a distinguishing characteristic of the h-BN spectrum, although, after careful calibration, a 0.1 eV shift of feature A to lower energy is observed when comparing the spectra of the films to that of the h-BN single crystal. As the surface roughness is increased, feature A—the signature of the π^* exciton—becomes more intense. Features B and C are a unique characteristic of the spectra of the c-BN films, and their intensity increases as the substrate becomes rougher. Since these features are found below the energy of the main onset of the absorption, it is likely that they are excitonic in nature.

Feature D, the first nonexcitonic feature of the c-BN crystal spectrum, is not very intense in the spectra of the films.

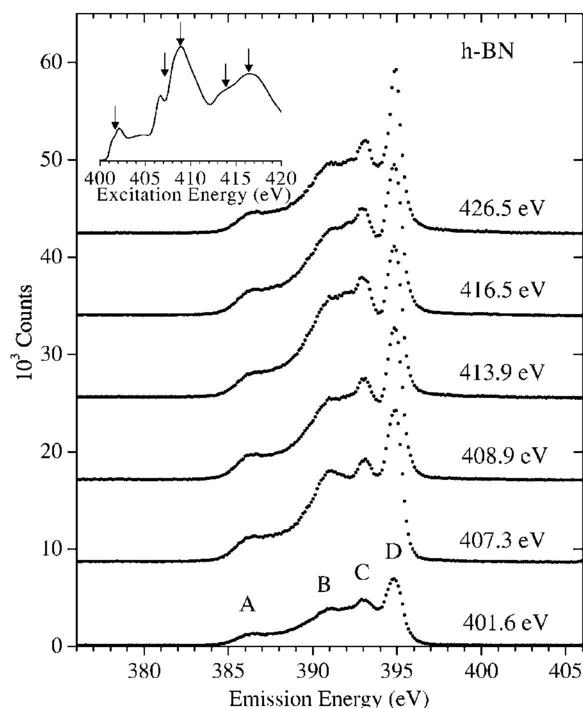

FIG. 5. Resonant nitrogen $K\alpha$ emission of h-BN. The inset displays the N 1s XAS spectrum and the excitation energies used for the resonant emission spectra.

The arrows associated with feature D are positioned at the first inflection point of the onset of the absorption into the conduction band. These locations were determined from the second derivatives of the spectra and shift by 0.2 eV upon

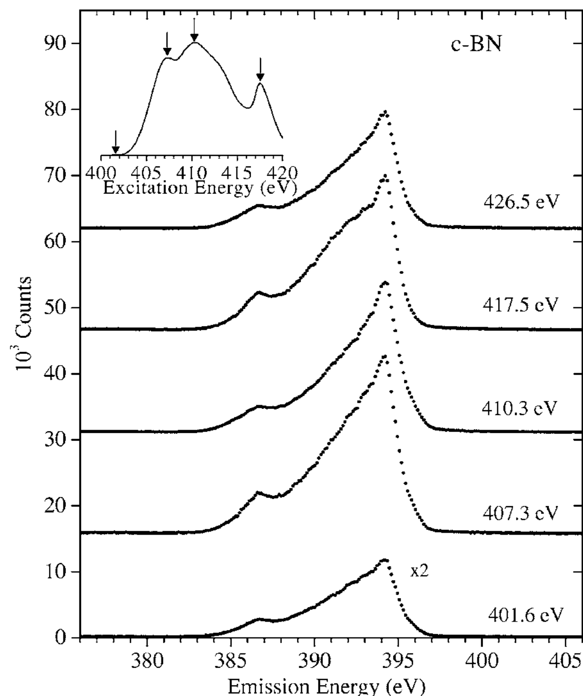

FIG. 6. Resonant nitrogen $K\alpha$ emission of c-BN. The inset displays the N 1s XAS spectrum and the excitation energies used for the resonant emission spectra.

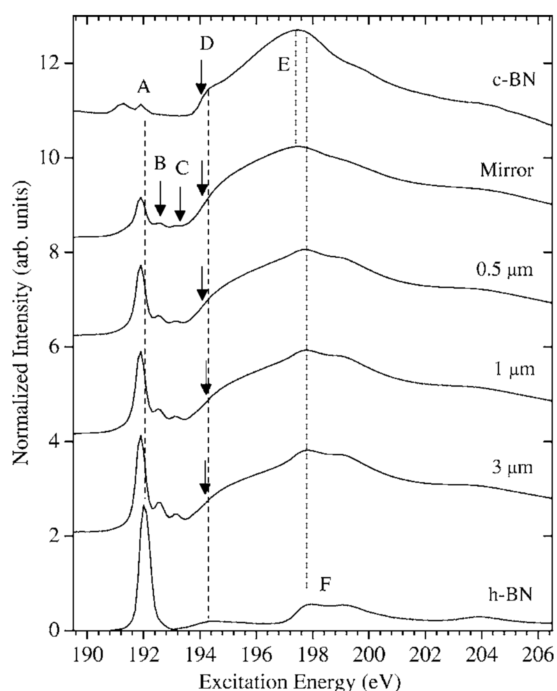

FIG. 7. Comparison of B 1*s* XAS of single crystals of *c*-BN and *h*-BN with *c*-BN thin films deposited on mirror silicon and scratched single crystal silicon wafers (silicon scratched with diamond particles of sizes of 0.25, 1, and 3 μm).

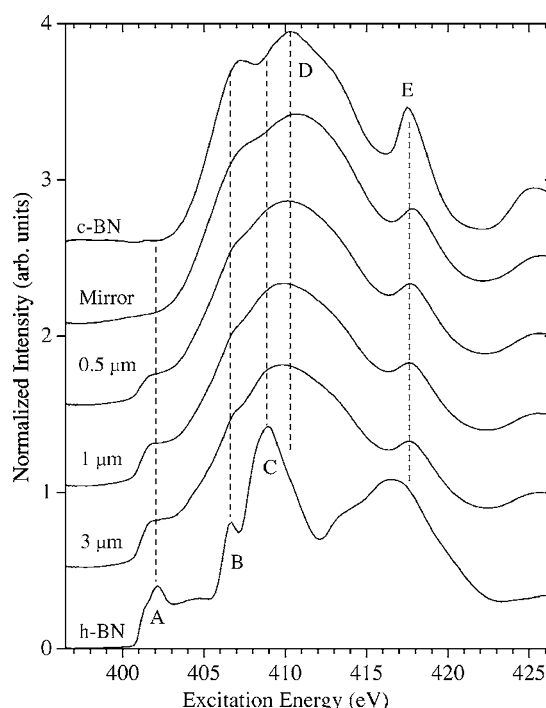

FIG. 8. Comparison of N 1*s* XAS of single crystals of *c*-BN and *h*-BN with *c*-BN thin films deposited on mirror silicon and scratched single crystal silicon wafers.

going from *c*-BN to the film grown on a surface scratched with 3 μm diamond particles. With the grain size on the nanometer scale, quantum confinement effects may be important when comparing the experimental results from the nanocrystalline films to those of the bulk crystal samples. The quantum confinement model predicts that the energies of the valence band and conduction bands may shift relative to the bands of the bulk sample, creating a larger band gap. X-ray spectroscopy has been used to show these effects in samples of Si and CdS nanocrystals.[45,46] The change in the inflection point on the onset of absorption indicates a change in the band structure of the films compared to the single crystal, possibly as a result of quantum confinement effects.

The most intense feature in the spectra of both the *c*-BN single crystal and the film grown on mirror silicon is feature E. In the spectra of the films deposited on scratched surfaces, however, the intensity is shifted 0.4 eV to higher energy, corresponding to a prominent feature in the *h*-BN spectrum (feature F). The presence of the *h*-BN-type features A and F in the thin film spectra indicates a mixture of sp^2 and sp^3 phases of nanocrystalline BN in the films. It is also clear that the amount of sp^2-bonded BN increases as the surface roughness is increased. There are clear variations in the boron 1*s* XAS spectra, not only between the spectra of the films and the single crystals, but also between the various films. The changes are a direct indication of differences in the electronic structures of the samples, the result of structural stress incurred during the growth process of the films on the varying surfaces and possibly of quantum confinement effects.

Figure 8 shows the nitrogen 1*s* XAS of the thin films and single crystals. As the roughness of the deposition surface is increased, there is a corresponding increase in the intensity of feature A in the spectra of the films. Feature A does not exist in the *c*-BN crystal, further confirming the presence of sp^2 phases in the films. Similarly, feature E is a distinguishing feature of the *c*-BN crystal spectrum, and it has a strong presence in the spectra of all the films, confirming that they also contain sp^3 phase BN (*c*-BN). The behavior of features B and C are further evidence that the sp^2 content increases with the surface roughness. Feature B does not exist in the *c*-BN spectrum but appears as a small shoulder in the spectrum of the films that were deposited on rougher substrates. In the *c*-BN crystal spectrum, feature D is prominent and, as the substrate becomes rougher, the intensity of feature A increases and the shoulders at features B and C become more noticeable, further indicating that the increase in substrate roughness produces a corresponding increase in the sp^2 bonded *h*-BN phase content of the films.

The comparisons between the XES spectra of the films also yield interesting results. Figure 9 displays the boron $K\alpha$ XES spectra measured at a resonant excitation energy. The spectra of the films are very similar to the spectrum of the *c*-BN single crystal. The *h*-BN spectrum measured at this excitation energy is very different from those of the *c*-BN crystal and the films.

The resonantly excited N $K\alpha$ XES spectra of the films are compared to those of the single crystals in Fig. 10. Not only do these spectra clearly show the presence of *h*-BN contaminant phases in the films, but they also further illustrate the immediate effects of scratching the substrate surface prior to growing the film. As would be expected from the analysis of the XAS spectra, the emission spectra of the films that were deposited on a previously scratched surface have a strongly defined peak structure that resembles that of *h*-BN, in con-

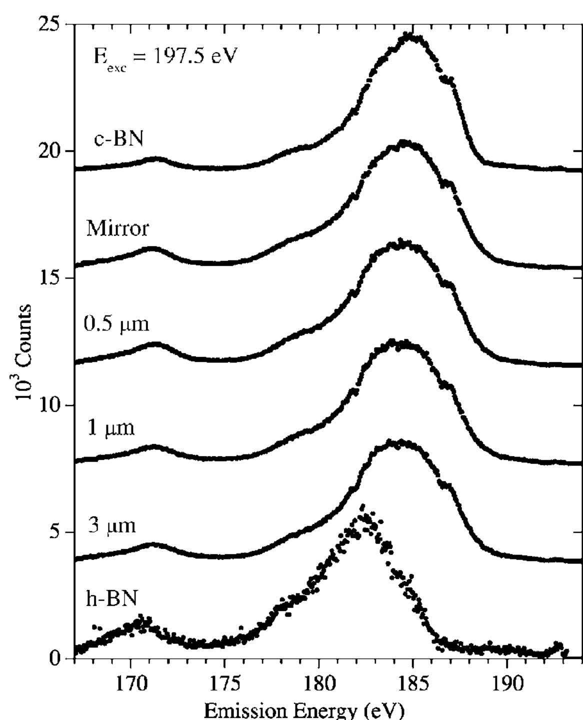

FIG. 9. Comparison of B $K\alpha$ XES of single crystals of *c*-BN and *h*-BN with *c*-BN thin films deposited on mirror silicon and scratched single crystal silicon wafers. The excitation energy was 197.5 eV.

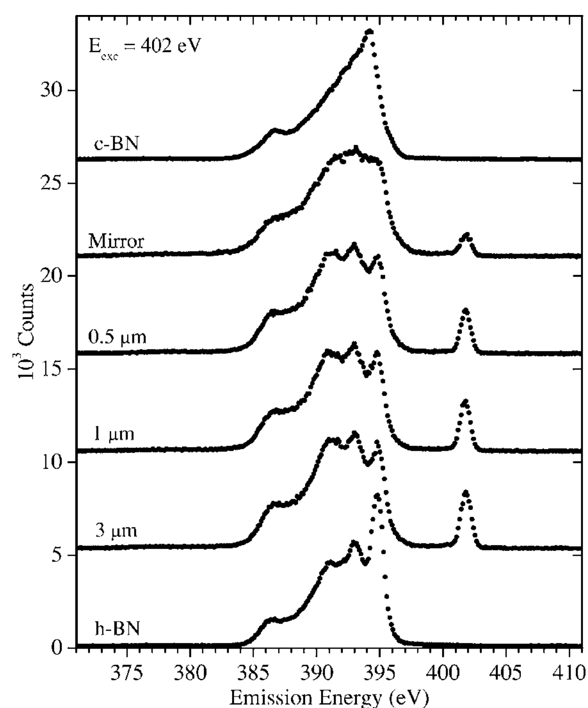

FIG. 10. Comparison of N $K\alpha$ XES of single crystals of *c*-BN and *h*-BN with *c*-BN thin films deposited on mirror silicon and scratched single crystal silicon wafers. The excitation energy was 402 eV.

trast with the spectrum measured from the film deposited on mirror silicon. It is also important to note that the XAS was measured in TEY, making it a fairly surface sensitive technique, while the XES measurements are more bulk sensitive. Both techniques show that the films are a mixture of *c*-BN and *h*-BN, as well as establishing the relationship between increasing substrate roughness and increasing sp^2 content.

VI. CONCLUSIONS

High-quality single crystals of *h*-BN and *c*-BN, as well as *c*-BN thin films deposited on silicon surfaces of varying roughness have been studied using x-ray absorption and x-ray emission spectroscopies. The spectra of the single crystals are compared to density of states calculations performed with density functional theory using the WIEN2K code. Good agreement is found when comparing the emission spectra measured at the boron and nitrogen edges with the 2*p* occupied partial DOS for *h*-BN and *c*-BN. The agreement between the XAS spectra and the unoccupied DOS would likely be improved by the inclusion of core hole effects in the calculations. The RIXS spectra for the single crystals are found to be to the same as previously reported measurements of crushed powder samples of *h*-BN and *c*-BN.

Differences in the electronic structure of the thin films, as compared to the single crystals, are revealed when comparing the XAS and XES spectra. These variations are likely the result of compressive stress during film deposition and possibly quantum confinement effects brought on by the small size of the particles in the nanocrystalline films. It is seen that the surface roughness of the substrate plays an important role in determining the structure of the resulting deposited film, in particular the sp^2/sp^3 bonding concentration. For the films deposited using the MSIBD technique, the ratio of the *c*-BN to *h*-BN phases decreases as the deposition surface becomes rougher. Soft x-ray spectroscopic techniques have proven to be an effective method for the detection of distinguishing spectral characteristics and changes in electronic structure in both single crystals and nanocrystalline thin films.

ACKNOWLEDGMENTS

Funding by the Natural Sciences and Engineering Research Council of Canada (NSERC) and the Canada Research Chair program is gratefully acknowledged. The work at the Advanced Light Source at Lawrence Berkeley National Laboratory was supported by U.S. Department of Energy (Contract No. DE-AC03-76SF00098).

[1] K. Watanabe, T. Taniguchi, and H. Kanda, Phys. Status Solidi A **201**, 2561 (2004).
[2] K. Watanabe, T. Taniguchi, and H. Kanda, Nat. Mater. **3**, 404 (2004).
[3] S. Shin, A. Agui, M. Fujisawa, Y. Tezuka, T. Ishii, Y. Minagawa, Y. Suda, A. Ebina, O. Mishima, and K. Era, Phys. Rev. B **52**, 11 853 (1995).
[4] P. Widmayer, H. Boyen, P. Ziemann, P. Reinke, and P. Oelhafen, Phys. Rev. B **59**, 5233 (1999).
[5] R. Wentorf, R. Devries, and F. Bundy, Science **208**, 873 (1980).
[6] C. Ronning, H. Feldermann, and H. Hofsass, Diamond Relat. Mater. **9**, 1767 (2000).
[7] L. Liu, Y. Feng, and Z. Shen, Phys. Rev. B **68**, 104102 (2003).
[8] L. Chkhartishvili, J. Solid State Chem. **177**, 395 (2004).
[9] Y. Xu and W. Ching, Phys. Rev. B **44**, 7787 (1991).
[10] A. Catellani, M. Posternak, A. Baldereschi, and A. Freeman, Phys. Rev. B **36**, 6105 (1987).
[11] J. Robertson, Phys. Rev. B **29**, 2131 (1984).
[12] V. Fomichev and M. Rumsh, J. Phys. Chem. Solids **29**, 1015 (1968).
[13] A. Mansour and S. Schnatterly, Phys. Rev. B **36**, 9234 (1987).
[14] W. OBrien, J. Jia, Q. Dong, T. Callcott, K. Miyano, D. Ederer, D. Mueller, and C. Kao, Phys. Rev. Lett. **70**, 238 (1993).
[15] A. Chaiken, L. Terminello, J. Wong, G. Doll, and C. Taylor, Appl. Phys. Lett. **63**, 2112 (1993).
[16] Y. Muramatsu, J. Kawai, T. Scimeca, M. Oshima, and H. Kato, Phys. Scr. **50**, 25 (1994).
[17] Y. Muramatsu, M. Oshima, J. Kawai, S. Tadokoro, H. Adachi, A. Agui, S. Shin, H. Kato, H. Kohzuki, and M. Motoyama, Phys. Rev. Lett. **76**, 3846 (1996).
[18] I. Jimenez, A. Jankowski, L. Terminello, J. Carlisle, D. Sutherland, G. Doll, J. Mantese, W. Tong, D. Shuh, and F. Himpsel, Appl. Phys. Lett. **68**, 2816 (1996).
[19] J. Jia, T. Callcott, E. Shirley, J. Carlisle, L. Terminello, A. Asfaw, D. Ederer, F. Himpsel, and R. Perera, Phys. Rev. Lett. **76**, 4054 (1996).
[20] D. Berns, M. Cappelli, and D. Shuh, Diamond Relat. Mater. **6**, 1883 (1997).
[21] I. Jimenez, A. Jankowski, L. Terminello, D. Sutherland, J. Carlisle, G. Doll, W. Tong, D. Shuh, and F. Himpsel, Phys. Rev. B **55**, 12 025 (1997).
[22] A. Agui, S. Shin, M. Fujisawa, Y. Tezuka, T. Ishii, Y. Muramatsu, O. Mishima, and K. Era, Phys. Rev. B **55**, 2073 (1997).
[23] J. Carlisle, E. Shirley, L. Terminello, J. Jia, T. Callcott, D. Ederer, R. Perera, and F. Himpsel, Phys. Rev. B **59**, 7433 (1999).
[24] N. Miyata, M. Yanagihara, M. Watanabe, Y. Harada, and S. Shin, J. Phys. Soc. Jpn. **71**, 1761 (2002).
[25] W. O'Brien, J. Jia, Q. Dong, T. Callcott, K. Miyano, D. Ederer, D. Mueller, and C. Kao, Phys. Rev. Lett. **70**, 238 (1993).
[26] P. B. Mirkarimi, K. F. McCarty, and D. L. Medlin, Mater. Sci. Eng., R. **21**, 47 (1997).
[27] T. Ikeda, Y. Kawate, and Y. Hirai, J. Vac. Sci. Technol. A **8**, 3168 (1990).
[28] L. Kleinman and J. Phillips, Phys. Rev. **117**, 460 (1960).
[29] A. Zunger, A. Katzir, and A. Halperin, Phys. Rev. B **13**, 5560 (1976).
[30] V. Solozhenko, A. Lazarenko, J. Petitet, and A. Kanaev, J. Phys. Chem. Solids **62**, 1331 (2001).
[31] T. Taniguchi, S. Koizumi, K. Watanabe, I. Sakaguchi, T. Sekiguchi, and S. Yamaoka, Diamond Relat. Mater. **12**, 1098 (2003).
[32] T. Taniguchi and S. Yamaoka, J. Cryst. Growth **222**, 549 (2001).
[33] O. Fukunaga, S. Nakano, and T. Taniguchi, Diamond Relat. Mater. **13**, 1709 (2004).
[34] H. Hofsass, C. Ronning, U. Griemeier, M. Gross, S. Reinke, and M. Kuhr, Appl. Phys. Lett. **67**, 46 (1995).
[35] N. Deyneka, X. Zhang, H. Boyen, P. Ziemann, and E. Banhart, Diamond Relat. Mater. **13**, 473 (2004).
[36] Q. Li, L. D. Marks, Y. Lifshitz, S. T. Lee, and I. Bello, Phys. Rev. B **65**, 045415 (2002).
[37] S. Weissmantel and G. Reisse, Diamond Relat. Mater. **10**, 1973 (2001).
[38] X. T. Zhou, T. K. Sham, C. Y. Chan, W. J. Zhang, I. Bello, S. T. Lee, and H. Hofsass (unpublished).
[39] J. J. Jia, T. A. Callcott, J. Yurkas, A. W. Ellis, F. J. Himpsel, M. G. Samant, S. Stöhr, D. L. Ederer, J. A. Carlisle, E. A. Hudson, L. J. Terminello, D. K. Shuh, and R. C. C. Perera, Rev. Sci. Instrum. **66**, 1394 (1995).
[40] J. Perdew, K. Burke, and M. Ernzerhof, Phys. Rev. Lett. **77**, 3865 (1996).
[41] P. Blaha, K. Schwarz, G. K. H. Madsen, D. Kvasnicka, and J. Luitz, *WIEN2k An Augmented Plane Wave+Local Orbitals Program for Calculating Crystal Properties*, Vienna University of Technology, Austria, Revised Edition, 2002.
[42] K. Schwarz, P. Blaha, and G. Madsen, Comput. Phys. Commun. **147**, 71 (2002).
[43] K. Schwarz and P. Blaha, Comput. Mater. Sci. **28**, 259 (2003).
[44] G. Mahan, Phys. Rev. B **21**, 1421 (1980).
[45] T. van Buuren, L. Dinh, L. Chase, W. Siekhaus, and L. Terminello, Phys. Rev. Lett. **80**, 3803 (1998).
[46] J. Lüning, J. Rockenberger, S. Eisebitt, J.-E. Rubensson, A. Karl, A. Kornowski, H. Weller, and W. Eberhardt, Solid State Commun. **112**, 5 (1999).